Nonleptonic Weak Decays of B to D$_s$ and D mesons

C. E. Thomas*

Rudolf Peierls Centre for Theoretical Physics, University of Oxford,
1 Keble Road, Oxford, OX1 3NP

(Dated: 23 March 2006)

Branching ratios and polarization amplitudes for B decaying to all allowed pseudoscalar, vector, axial-vector, scalar and tensor combinations of D_s and D mesons are calculated in the Isgur Scora Grinstein Wise (ISGW) quark model after assuming factorization. We find good agreement with other models in the literature and the limited experimental data and make predictions for as yet unseen decay modes. Lattice QCD results in this area are very limited. We make phenomenological observations on decays in to $D_s(2317)$ and $D_s(2460)$ and propose tests for determining the status and mixings of the axial mesons. We use the same approach to calculate branching ratios and polarization fraction for decays in to two D type mesons.

PACS numbers: 13.25.Hw, 12.15.Ji, 12.39.Jh

I. INTRODUCTION

Non-leptonic weak decays of B-mesons are important because they probe both electroweak physics and hadronic structure, and may provide a window on physics beyond the standard model. As well as its intrinsic interest, the hadronic part must be understood in order to extract electroweak and new physics from these decays. This involves non-perturbative QCD and so can not be calculated from first principles. There have been many attempts to model the hadronic part and their success varies depending on which decay mode is studied. There are only very limited lattice QCD results in this area. Semi-leptonic decays of B and D mesons have been successfully studied using the Isgur Scora Grinstein Wise (ISGW) model [1]. We extend this model to the study of exclusive non-leptonic decays after assuming factorization of these decays. The model has corrections that vanish when the final mesons have zero recoil and so should be most reliable close to this kinematic region.

Heavy Quark Effective Theory (HQET) as used, for example, in Ref. [2], provides a set of symmetry relations but not expressions for the rates. Some explicit model must still be used. The ISGW model satisfies the requirements of HQET in the zero recoil limit [3] and provides an explicit model in which calculations can be made.

There are also pole models such as that of Bauer, Stech & Wirbel (BSW) [4][5] which we compare to our results. There are different approaches for heavy to light decays such as the Soft Collinear Effective Theory (SCET) framework [6] and Light-Cone Sum Rules [7][8]. These are useful where the final state mesons have high energy unlike the regime close to zero recoil that we are probing here.

Some predictions have been made for decays to combinations of pseudoscalar D_s and D and vector D_s^* and D^* such as by Luo & Rosner [2] and Chen et. al. [9]. Datta and O'Donnell [10] have made limited studies of the decays to axial and scalar D_s. Cheng et. al. in Ref. [11] have studied s and p-wave form factors in the light-front approach. They have compared this to improved ISGW model [3] results given in Ref. [12]. We specialize to the D_s D modes where the ISGW predictions should be reliable and calculate explicit results for all possible combinations of p and s-wave mesons consistently in one model giving polarization ratios where applicable.

With B factories tightening current observations of B decays and finding new decay modes it is timely that these modes should be studied in detail.

Our aims are to:

- Provide robust predictions of branching ratios and polarization fractions for all the possible combinations. These can be compared with current and future experimental data.

- Comment on what can be learnt about the nature of $D_s(2317)$ and $D_s(2460)$ mesons and axial vector mixing.

We start in Section II with a discussion of factorization and general remarks. In Section III we briefly describe the ISGW model and extend it to non-leptonic decays after assuming factorization. In Section IV we present our results for the branching ratios and polarization fractions of the allowed decay modes. We also compare our results with those from other models and experimental data in this section. Then we apply the same method to decays in to two D type mesons. In Section V we discuss what we can learn about the scalar and axial D_{s0} and D_{s1}. We finish with some general remarks and conclusions in Section VI and suggest some experimental observations that could be made.
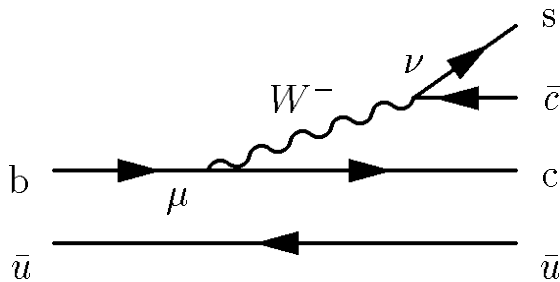
*E-mail: c.thomas1@physics.ox.ac.uk

FIG. 1: $B^-(b\bar{u}) \to D_s^-(\bar{c}s)D^0(c\bar{u})$ - Type I Tree Diagram

II. GENERAL DEFINITIONS AND FACTORIZATION

The color favored tree diagram ("Type I tree diagram") for $B \to D_s D$ is shown in Fig. 1. Here D_s and D can be any s or p-wave $s\bar{c}$ and $c\bar{u}$ states. We ignore any contribution to this process from penguin and weak-annihilation topologies.

The rate for a general Type I Tree decay $B(b\bar{q}_i) \to Y(q_1\bar{q}_2)X(q\bar{q}_i)$ (e.g. $Y = D_s$ and $X = D$) can be written as:

$$\Gamma = \frac{G_F^2}{16\pi} a_1^2 |V_{qb}V_{q_1 q_2}|^2 \frac{|\mathbf{q}|}{M_B^2} |A|^2. \qquad (1)$$

where G_F is the Fermi Constant, a_1 is the effective Wilson coefficient, V_{qb} and $V_{q_1 q_2}$ are Cabibbo-Kobayashi-Maskawa (CKM) quark-mixing matrix elements, $\mathbf{q}$ is the recoil 3-momentum in the rest frame of B and M_B is the B-meson mass. $|A|^2$ is the sum of the squares of the polarization amplitudes A_i:

$$|A|^2 \equiv \sum_i |A_i|^2. \qquad (2)$$

We use the notation $i = +-$, $-+$ or ll where the first label denotes the helicity of the X meson.

We follow Rosner & Luo [2] by assuming the factorization hypothesis (naive factorization) and writing the amplitude as a product of two matrix elements:

$$A_i = <Y|J_\mu|0><X|J^\mu|B>, \qquad (3)$$

where $J_\mu \equiv V_\mu - A_\mu \equiv \bar{q}_f \gamma_\mu(1 - \gamma_5)q_i$ is the vector-axial current. In QCD Factorization [13] [14] [15] it has been shown that B decays to two heavy mesons do not obey the BBNS factorization formula and so naive factorization is not expected to hold. However, as noted in Ref. [14], the charm quark mass is at an intermediate scale between the light and heavy (bottom quark mass) scales

and so factorization is still an open question in the modes we consider. Empirically factorization works where it has been tested in these modes [2] [16] [9]. Comparison of our results with experiment can further test this assumption. The effective Wilson coefficient a_1 contains some QCD corrections. As remarked in Ref. [2] this varies from process to process but only by less than about 1%. We therefore use that paper's value, $a_1 = 1.05$, for all processes.

The matrix element $< X|J^\mu|B >$ can be parameterized in terms of general form factors. We use the same definitions as ISGW and these are given in Appendix A. These form factors can then be calculated in a particular model such as ISGW discussed in Section III. The polarization vectors and tensors used for $J = 1$ and $J = 2$ mesons are given in Appendix B.

The matrix element $< Y|J_\mu|0 >$ can be parameterized in terms of the decay constant of meson Y, f_Y. For vector ($^3S_1$) and axial vector ($^3P_1$, $^1P_1$) mesons [44] with polarization vector ϵ_μ^Y and mass M_Y this is defined by

$$< Y|J_\mu|0 >= \epsilon_\mu^{*Y} f_Y M_Y, \qquad (4)$$

and for scalar ($^3P_0$) and pseudoscalar ($^1S_0$) mesons [45] with 4-momentum P_μ^Y,

$$< Y|J_\mu|0 >= iP_\mu^Y f_Y. \qquad (5)$$

III. THE ISGW MODEL

The ISGW model [1] was developed to calculate semileptonic B and D decays using a constituent quark model and the mock meson approach [17]. We extend the model to non-leptonic decays using the factorization hypothesis and test the sensitivity to the assumptions made. We find that robust predictions can be made for the D_s D decay modes because they are in the valid kinematic region.

The matrix element $< X|J^\mu|B >$ is calculated using a non-relativistic decomposition of the quark current $\bar{q}\gamma_\mu(1 - \gamma_5)b$. This will contain corrections of $O(|\mathbf{q}|^4/m_{q_i}^4)$ and $O(|\mathbf{q}|^4/M_X^4)$ where m_{q_i} are the quark masses appearing in the current decomposition. The model is therefore reliable only close to zero recoil and with heavy quarks. M_B is the mass of the B meson, M_X is the mass of the D (or excited D) meson, M_Y is the mass of the D_s (or excited D_s) meson. $\tilde{M}_B$, $\tilde{M}_X$ and $\tilde{M}_Y$ are the respective mock meson masses. P_B, P_X, P_Y are the 4-momenta, $y \equiv \frac{t}{M_B^2} \equiv \frac{(P_B - P_X)^2}{M_B^2} = \frac{M_Y^2}{M_B^2}$, and $t_m \equiv \max t = (M_B - M_X)^2$. The quarks are the spectator antiquark $\bar{q}_i$, the decaying quark b, the quark in the final state meson with the spectator quark q, and the quark and antiquark pair in the other final state meson q_1 and $\bar{q}_2$. m_{qi}, m_b, m_q, m_{q1} and m_{q2} are the constituent quark masses. In the decay $B^- \to D_s^- D^0$: $\bar{q}_i = \bar{u}$, $q = c$, $q_1 = s$ and $\bar{q}_2 = \bar{c}$.

In the original ISGW paper the semileptonic differential rate is given in terms of the form factors. We have adapted the model to calculate non-leptonic decays in the factorization hypothesis given above. The resulting relationships between polarization amplitudes, form factors and decay constants are given in Appendix C. For connection with the original ISGW paper [1], their hadronic tensor (Equ. 7) is given by

$$h_{\mu\nu} = \sum_i <B|J_\nu^\dagger|X><X|J_\mu|B> . \qquad (6)$$

We initially followed the original ISGW paper using (radial ground state) harmonic oscillator (HO) wavefunction of the momentum space form:

$$\psi_{l=0,m_l=0}(\mathbf{k}) = \left(\pi\beta^2\right)^{-3/4} \exp\left(-\frac{|\mathbf{k}|^2}{2\beta^2}\right), \quad (7)$$

$$\psi_{l=1,m_l=0(1)}(\mathbf{k}) = \sqrt{2}\left(\pi\beta^2\right)^{-3/4} \frac{k_{z(+)}}{\beta} \exp\left(-\frac{|\mathbf{k}|^2}{2\beta^2}\right). \quad (8)$$

where β is the wavefunction parameter and $k_+ = -\frac{1}{\sqrt{2}}(k_x + ik_y)$. The wavefunctions are normalized such that $\int d^3k\psi^*(k)\psi(k) = 1$.

The resulting ISGW form factors using harmonic oscillator (HO) wavefunctions are given in Appendix D. These are mostly the same as the ISGW paper with some additional ones not given in that paper. However, there are a couple of differences. The sign of the scalar form factor u_+ in Equ. D14 is opposite to that in Equ. B37 of Ref. [1]. As Ref. [1] does not give an expression for u_- it is not possible to tell if this is an overall or relative sign. It seems likely that it is an overall sign due to the conventions used, in which case it has no affect on the results. If it is a relative sign it can only modify the results when meson Y is a pseudoscalar or scalar. If, for example, Y is the pseudoscalar D_s, adding a relative sign changes the branching ratio significantly: from 4.2×10^{-4} to 2.2×10^{-3}.

The other difference is the additional mass ratio $\tilde{M}_B/\tilde{M}_X \approx 2.2$ in the axial vector (1^{+-}) form factor v in Equ. B43 of Ref. [1] compared with Equ. D11 here. This is a parity violating form factor which appears in decays where meson Y is a vector or an axial vector and only in the transverse polarization amplitudes. This has a negligible affect on the branching ratios and longitudinal fractions. For example, when Y is the vector D_s^*, the branching ratios (arbitrary normalization) are $\propto 5.28 \times 10^{13}$ and 5.29×10^{13}, and the longitudinal fractions 0.930 and 0.928 respectively without and with the mass ratio. However, there is a significant affect on the parity odd fraction $\propto (A_{+-} - A_{-+})^2$. This is 0.66×10^{-3} without the mass ratio but 3.1×10^{-3} with it.

The original ISGW paper was restricted to harmonic oscillator wavefunctions; our ISGW form factors for general wavefunctions are given in Appendix E.

In the original ISGW paper $|\mathbf{q}|^2$ in form factors is approximated as $(t_m - t)M_X/M_B$ and a relativistic correc-

Quark	Constituent Quark Mass / MeV
b	5170
$q = q_1 = c$	1770
$q_i = u$	330
$q_2 = s$	550

TABLE I: Constituent quark masses [18].

tion factor κ is introduced through $|\mathbf{q}|^2 \to |\mathbf{q}|^2/\kappa^2$. This was intended to bring the pion form factor into better agreement with experiment at the low q^2 region [1]. We take $\kappa = 0.75$ [18]. However, we look at how much κ influences the results by setting $\kappa = 1$ in one model.

There is ambiguity in the mock meson approach [19] as to whether, at the end of the calculation, to identify the mock meson masses as the physical meson masses or the sum of the constituent quark masses.

We used a number of different models corresponding to different choices to assess the robustness of the approximations used. In model 1 the $(t_m - t)$ form is used in place of $|\mathbf{q}|^2$. In models 2 and 3 the exact $|\mathbf{q}|^2$ is used in the exponential of F_3. In models 1-2 the mock meson masses are equal to the physical meson masses. In model 3 the physical meson masses are used except in the exponential of F_3 where the sum of the constituent quark masses is used. Models 4-5 take the mock meson masses to be the sum of the constituent quark masses. Model 4 uses $(t_m - t)$ and model 5 uses $|\mathbf{q}|^2$. Model 6 is the same as model 3 except that we set $\kappa = 1$.

The D_s D decay mode is expected to be reasonably well modeled by ISGW. The highest recoil momentum (that for final state pseudoscalars) is 1812 MeV. $|\mathbf{q}|/m_b \approx 0.35$, $|\mathbf{q}|/m_c \approx 1.02$, $|\mathbf{q}|/M_D \approx 0.97$. Although $|\mathbf{q}|/m_c$ and $|\mathbf{q}|/M_D$ do not appear small, they appear as, for example, $|\mathbf{q}|^4/(8M_D^4)$ in a Taylor expansion with numerical value ≈ 0.14. The approximation is therefore reasonable. In the following section we present the results of our calculation.

IV. RESULTS OF CALCULATIONS

A. ISGW Model Results

Unless otherwise stated all numerical values of constants, masses etc. are taken from the PDG Review 2004 [23]. The quark masses and HO wavefunction parameters used are shown in Tables I and II respectively. We take $a_1 = 1.05$ [2], $|V_{bc}| = 0.04$ and $|V_{cs}| = 0.97$. The magnitudes of decay constants used are given in Table III. The phases of the decay constants are chosen to match those given by quark model calculations in Appendix F.

To be explicit, we consider the mode in which a charged B decays in to a charged D_s and neutral D^0. Initially

Meson	β / MeV
B	410
D	390
D^*	390
D_0	330
D_1	330
D_2	330

TABLE II: HO wavefunction parameters [20].

Meson	Decay Constant f / MeV
D_s	240 MeV [21]
D_s^*	275 MeV [21]
D_{s0}	110 MeV [22]
$D_{s1}1$	240 MeV [22]
$D_{s1}2$	63 MeV [22]

TABLE III: D_s meson decay constants.

we take the axial vector $D_{s1}(2460) \equiv D_{s1}1$ to be $^3P_1$ with mass 2460 MeV. The $D_{s1}(2536) \equiv D_{s1}2$ is $^1P_1$ and has mass 2536 MeV. We discuss axial vector mixing in Section V. The scalar D_{s0} is assumed to be the $D_s(2317)$ with mass 2317 MeV. We take both axial D_1 to have mass 2420 MeV: $D_1 1$ is $^3P_1$ and $D_1 2$ is $^1P_1$. The scalar D_0 has mass 2350 MeV and the tensor D_2 has mass 2459 MeV.

As discussed in Section III, to get a handle on the theoretical uncertainty within the ISGW model, we calculated the branching ratios and polarization ratios using six different model choices.

A plot of the calculated decay rates and the experimental results is shown in Fig. 2. The model error bars and average show the range and average of the six model choices. The experimental results are from the PDG Review 2004 [23] apart from: $B^0 \to D_s^+ D^-$ which is from

Belle [24] and $B^0 \to D_s^{*+} D^{*-}$ which is from BABAR [25]. Tables of numerical results are given in Tables V and VI of Appendix G. Products of branching ratios have been measured for the $D_s(2317)$ and $D_s(2460)$ modes from BABAR [26] and Belle [27]. This data is averaged in the PDG Review 2005 Partial Update [28] and discussed in Section V.

Where data exist the model seems in remarkable agreement. The possible exceptions are the newer Belle and BABAR results for the neutral B decaying to $D_s^- D^+$ and $D_s^{*-} D^{+*}$. Both these neutral B modes are lower than the model predictions and, although this is not significant, they are lower than the corresponding charged B mode. If more precise data shows a discrepancy between charged and neutral decays it would be due to some difference between u and d spectator quarks. Spectator interaction effects which could cause this include weak annihilation, which can only contribute to the charged B^+ decay, and electromagnetic penguins.

The variation due to the model choice is relatively small; it's of the same order or less than the experimental uncertainty for those modes with experimental data. This suggests the predictions made are robust. The model uncertainty shown does not include uncertainty in the decay constants: this would change the overall branching ratio for each Y (e.g. D_s) meson but not the pattern for a given Y.

The $D_{s1}1$ D^*, $D_{s1}1$ D and $D_{s1}2$ D^* modes are relatively large but are complicated by axial vector mixing. We comment on implications for D_{s0} and D_{s1} mesons in Section V.

Polarization ratios for the relevant decay modes are shown in Fig. 3. There is only one piece of experimental data in the PDG Review 2004: that from BABAR and CLEO on the decay in to D_s^* D^*. Here there is good model agreement. The model uncertainty is $\sim 10\%$ being slightly larger for the $D_1 1$ modes. Again the model predictions are robust.

We then looked at the ISGW model with more realistic wavefunctions using the results of Appendix E and a numerical solution of the radial Schrödinger equation. This was done by discretizing the position coordinate in to 300 intervals ranging from 0 to $\approx 2 \times 10^{-2} \mathrm{MeV}^{-1}$. We first checked our numerical method by solving a HO potential $V = 1/2\mu\omega^2 r^2$ where $\omega = \beta^2/\mu$ and μ is the reduced mass of the quarks. The results were the same as the HO analytic ones to the numerical accuracy.

We then used a more realistic Linear + Coulomb + Hyperfine (LCHF) potential with the delta function smoothed out to a Gaussian [29][30]:

$$V = -\frac{4}{3}\frac{\alpha_s}{r} + br + \frac{32\alpha_H\sigma^3}{9m_q m_{\bar{q}}\sqrt{\pi}}\left(\mathbf{s_q} \cdot \mathbf{s_{\bar{q}}}\right)\exp\left(-\sigma^2 r^2\right). \quad (9)$$

Taking $\alpha_s = 0.594$, $b = 1.62 \times 10^5 \mathrm{MeV}^2$, $\sigma = 897\mathrm{MeV}$ and $\alpha_H = \alpha_s$. The resulting form factors are negligibly different from the HO ones compared with the other model uncertainties. Varying the parameters in the LCHF potential by 10% leads to negligible changes in the results.

So, to summarize, the potential used does not appear to modify our results significantly.
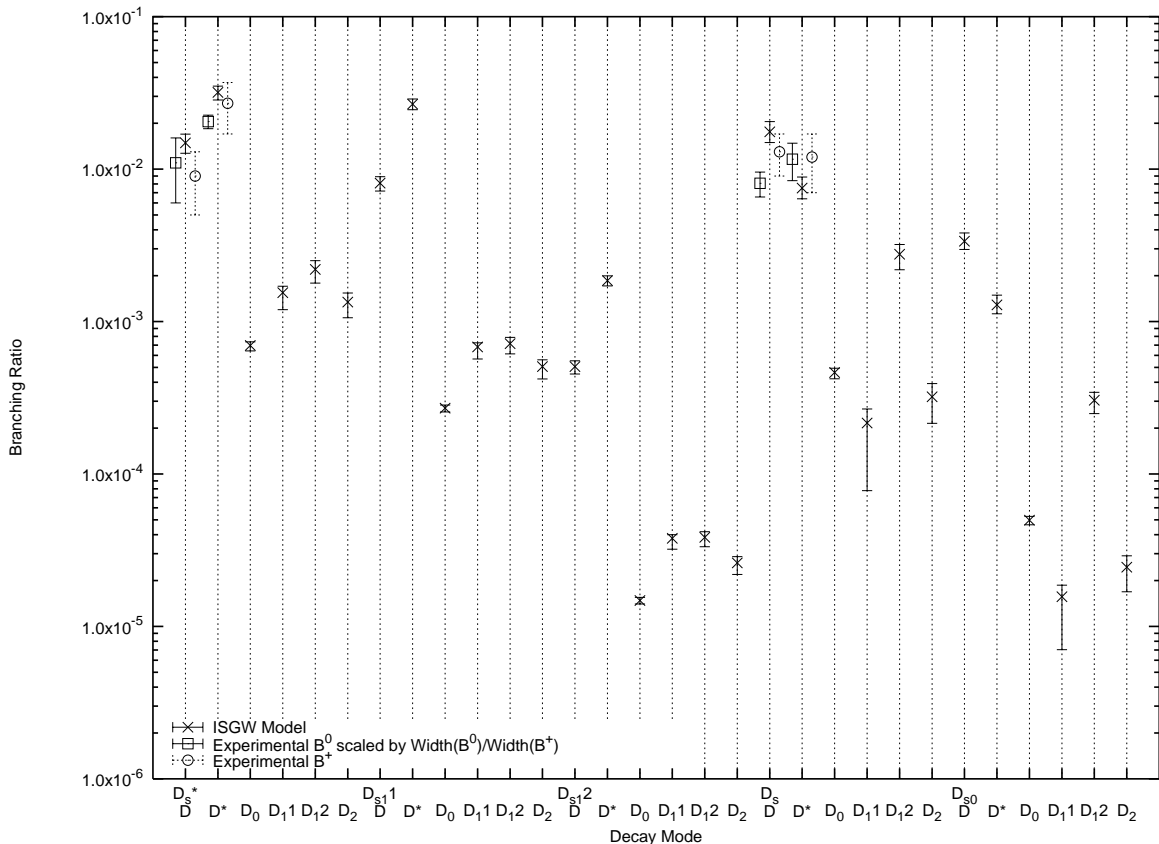
FIG. 2: $B \to D_s D$ Branching Ratios: ISGW model and experimental values. See the text for references to experimental results.

B. Comparison with Other Results

We compared these results with calculations based on the BSW model [4][5], Luo and Rosner's HQET based model in ref. [2] and the pole model in that reference. We used our values of the masses, decay constants, CKM matrix elements and a_1. These models only allow predictions when meson X is a vector or pseudoscalar meson. The branching fraction results are shown in Fig. 4 and the polarization ratios in Fig. 5. It can be seen that there is reasonably good agreement between the four models. This adds to our confidence in the robustness of our results. The ISGW model appears to give a slightly worse fit in some cases. However we should note that we haven't fitted anything to these decays. The only parameter, a_1, was obtained for general B decays.

Cheng et. al. [11] have used a light-front approach to calculate some of these decay modes. They do not, however, give explicit results for all the modes that can be compared to experimental data. The light front approach has the advantage of being relativistic, however, in the region close to zero recoil being studied we have argued that the ISGW model should be valid. The light front approach uses a parameterization to get from maximum recoil to the physical regime.

Cheng [12] has also studied s and p-wave form factors in an improved ISGW model [3]. However different models are used for different transitions. For consistency we have used the same model for all the decay modes. We give explicit results for all possible combinations including p-wave and and p-wave modes some of which are comparable in magnitude to the p-wave + s-wave modes. We present polarization ratios where appropriate. None of the parameters have been fit to these decays; the decay constants are determined from other experimental results or models. We have also attempted to assess the impact of some of the approximations in our results. Their qualitative pattern is the same as ours but there are quantitative differences, comparison being complicated by mixing effects.

Lattice calculations currently only determine the form factors at zero recoil for semileptonic decays of B to D or D^*. Therefore branching ratios can not be compared with our calculations. For $B \to D$ the lattice results are given as $F(w = 1)$ where $w = P_B \cdot P_X / (M_X M_B)$. This is related to the ISGW form factor f_+ by

$$F = \frac{2\sqrt{M_X M_B}}{M_X + M_B} f_+. \tag{10}$$

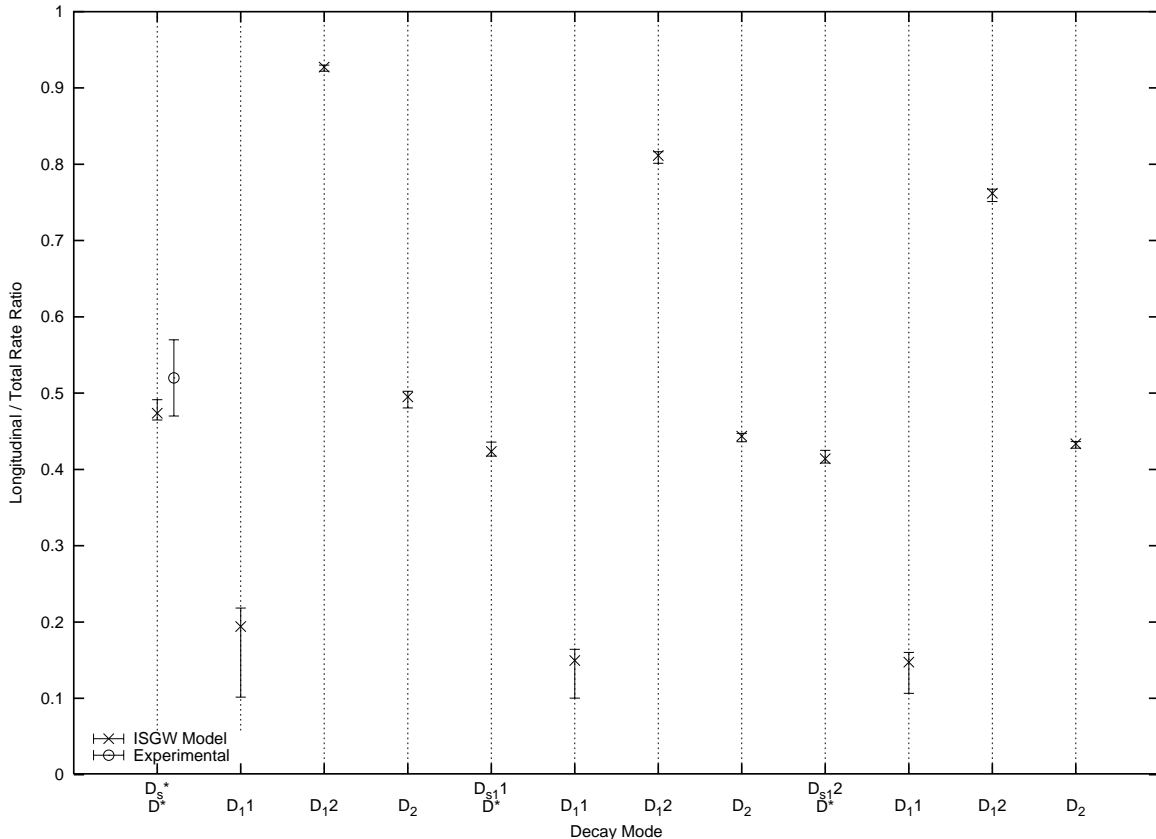The ISGW model gives 0.961 to 1.02 depending on what

FIG. 3: Polarization Ratios: ISGW model and experimental values. See the text for references to experimental results.

masses are used for the mock meson masses. Lattice calculations give $1.074 \pm 0.018 \pm 0.016$ [31]. For $B \to D^*$ the lattice results are given as $F_A(w = 1)$. This is related to the ISGW form factor f by

$$f = \sqrt{M_X M_B} F_A(w)(1 + w). \qquad (11)$$

The ISGW model gives this as 0.998 whereas a quenched lattice calculation gives $0.913^{+0.024}_{-0.017} \pm 0.016^{+0.003+0.000+0.006}_{-0.014-0.016-0.014}$ [32]. In both cases the results of lattice and ISGW models differ.

C.   The $B \to DD$ Modes

The ISGW model can also be used in decays to two D (and excited) mesons. The dominant contribution is again expected to be from the Type I tree diagram shown in Fig. 1. In the decay $B^- \to D^- D^0$: $\bar{q}_i = \bar{u}$, $q = c$, $q_1 = d$ and $\bar{q}_2 = \bar{c}$. These decays are Cabibbo suppressed with the CKM matrix element V_{cs} replaced by V_{cd} leading to a suppression factor of 0.05 in rate compared with the $D_s D$ modes. This means that other contributions may be relatively more important.

An additional complication is in distinguishing the two D mesons produced. In neutral B decays the B^0 and $\bar{B}^0$ decays must be distinguished to determine which D meson is which. In the B^0 decay meson Y has charge $+$ whereas in the $\bar{B}^0$ decay it has charge $-$. This is not a problem in charged B decays where meson Y is always charged and X is neutral.

With these caveats the decays can be calculated as above. We take $|V_{cd}| = 0.22$. The magnitudes of decay constants used are given in Table IV. These are from a quark model calculation using HO wavefunctions, as described in Appendix F, normalized to the f_D result from CLEO [33]. They produce the same pattern of results as in Ref. [22].

Meson	Decay Constant f / MeV
D	223 [33]
D^*	215
D_0	156
$D_1 1$	183
$D_1 2$	89

TABLE IV: D meson decay constants

The branching ratios and polarization fractions are shown Figures 6 and 7 respectively. Numerical values are given in Tables VII and VIII of Appendix G. In the
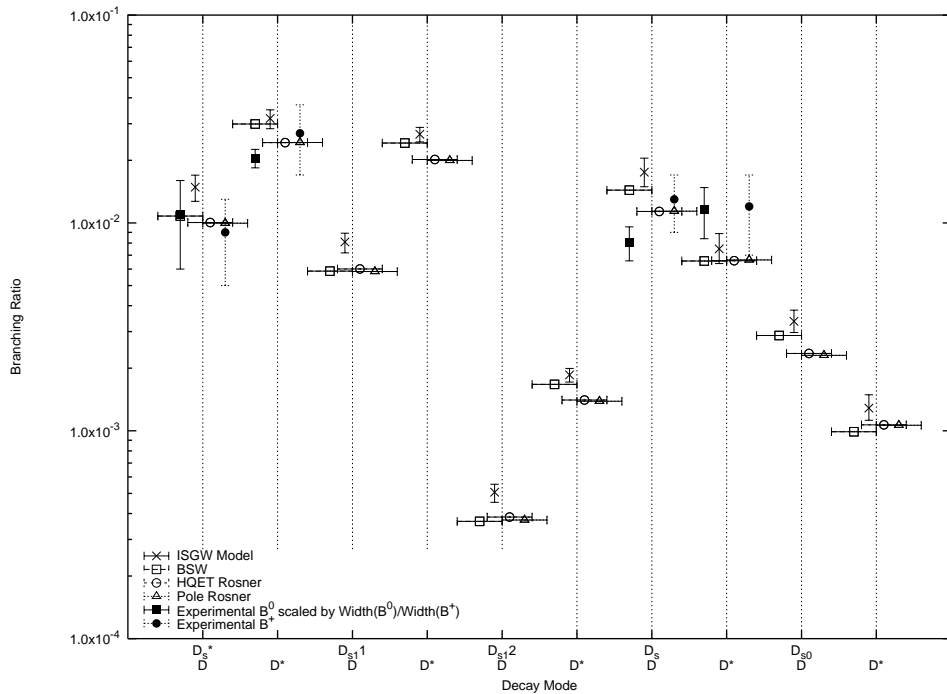
FIG. 4: $B \to D_s D$ Branching Ratios: Different models. Experimental data as in Fig. 2.
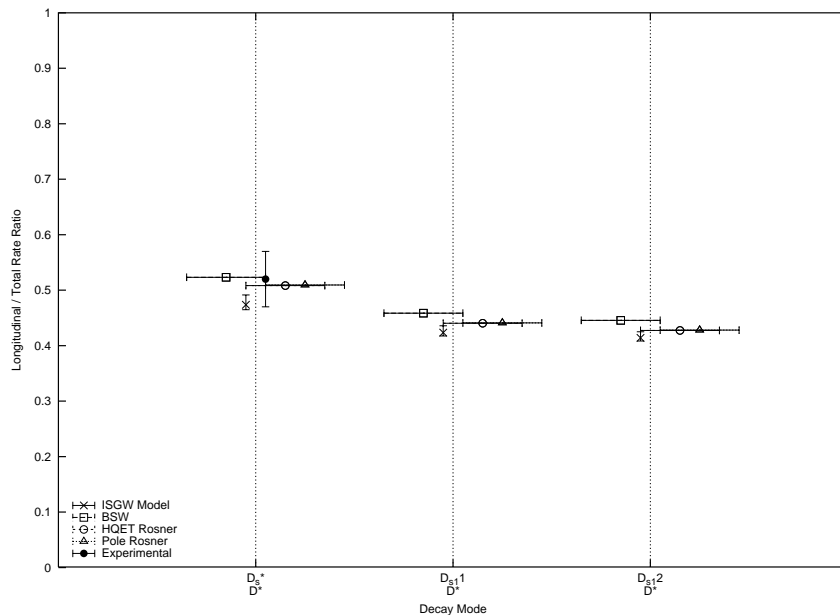

FIG. 5: Polarization Ratios: Different models. Experimental data as in Fig. 3.

PDG Review 2005 Update [28] there are only upper limits for the vector and pseudoscalar modes along with a combined branching ratio in to $D^+ D^*$ and $D^{*+} D$ of $0.93 \pm 0.15 \times 10^{-3}$. The experimental data shown on the figures is from Belle [34] [35]. There is good agreement except for decay to D D. Again here the B^0 branching ratio is lower than the B^+ branching ratio. The model uncertainty shown does not include uncertainty in the decay constants which could be significant.

Because of the charge conjugation symmetry of the final state in decays to $D^* \bar{D}^*$ another interesting observable is the CP odd fraction, $R_\perp$. This is related to the helicity amplitudes: Equs. C4 and C5 in Appendix C by

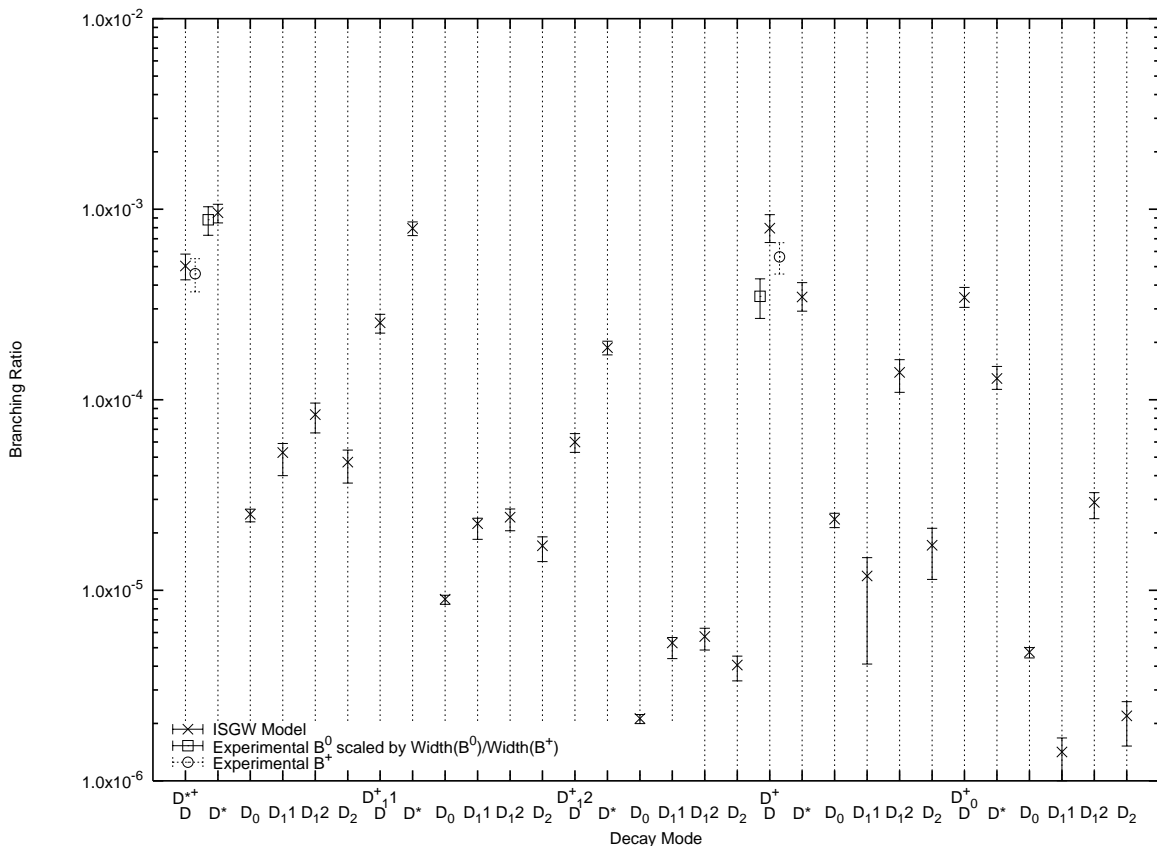$$R_\perp = \frac{|A_{+-} - A_{-+}|^2}{2(|A_{+-}|^2 + |A_{-+}|^2 + |A_{ll}|^2)} \quad (12)$$

FIG. 6: $B \to DD$ Branching Ratios: ISGW model and experimental values. See the text for references to experimental results.

The model $R_\perp$ are shown in Table IX of Appendix G. There is experimental data on $R_\perp$ in the decay to D^*D^*: Belle gives $R_\perp = 0.19 \pm 0.08 \pm 0.01$ [34] and BABAR $R_\perp =$ 0.125 ± 0.044 ± 0.007 [36]. This is in general agreement with $R_\perp = 0.086$ from the ISGW model.

Chen et. al. in ref. [9] have used generalized factorization to study decays to pseudoscalar and/or vector D mesons and compared a number of approaches. They include penguin and annihilation effects and comment that penguin effects are not negligible in decays to two pseudoscalars. They have better agreement with experiment in that mode and so this could be a contribution to the discrepancy between our branching ratio to $D\,D$ and experiment.

V. PHENOMENOLOGICAL IMPLICATIONS FOR D_{s0} AND D_{s1}

The $D_s(2317)$ (0^+) and $D_s(2460)$ (1^+) do not fit easily in to the $c\bar{s}$ spectroscopy [37]. These states could be conventional $c\bar{s}$ mesons with lower than expected masses [38]. Alternatively they could be multiquark or molecular mesons associated with DK and D^*K thresholds [39].

Measuring branching ratios to D or D^* with $D_s(2317)$ or $D_s(2460)$ would help determine the nature of these mesons. If the measured branching ratios are consistent with our predictions this would support them being conventional mesons. If this is the case, the mixing angle of the $^3P_1$ and $^1P_1$ states in to physical axial vector mesons $D_s(2460)$ and $D_s(2536)$ can also be determined.

Products of branching ratios have been measured for the $D_s(2317)$ and $D_s(2460)$ modes from BABAR [26] and Belle [27] and included in the PDG Review 2005 Partial Update [28]. Following Datta and O'Donnell [10] we estimate lower limits for modes containing these mesons.

For decays to $D_s(2317)\,D$ we get experimental lower limits of $(9.0 \pm 3.2) \times 10^{-4}$ for the B^+ decay and $(1.1 \pm 0.4) \times 10^{-3}$ for the B^0 decay. For decays to $D_s(2317)\,D^*$ we obtain $(9\pm7)\times10^{-4}$ and $(1.5\pm0.6)\times10^{-3}$ respectively. These are consistent with the model predictions.

We parameterize the mixing of the axial D_s states in terms of a mixing angle ϕ. The physical states are then
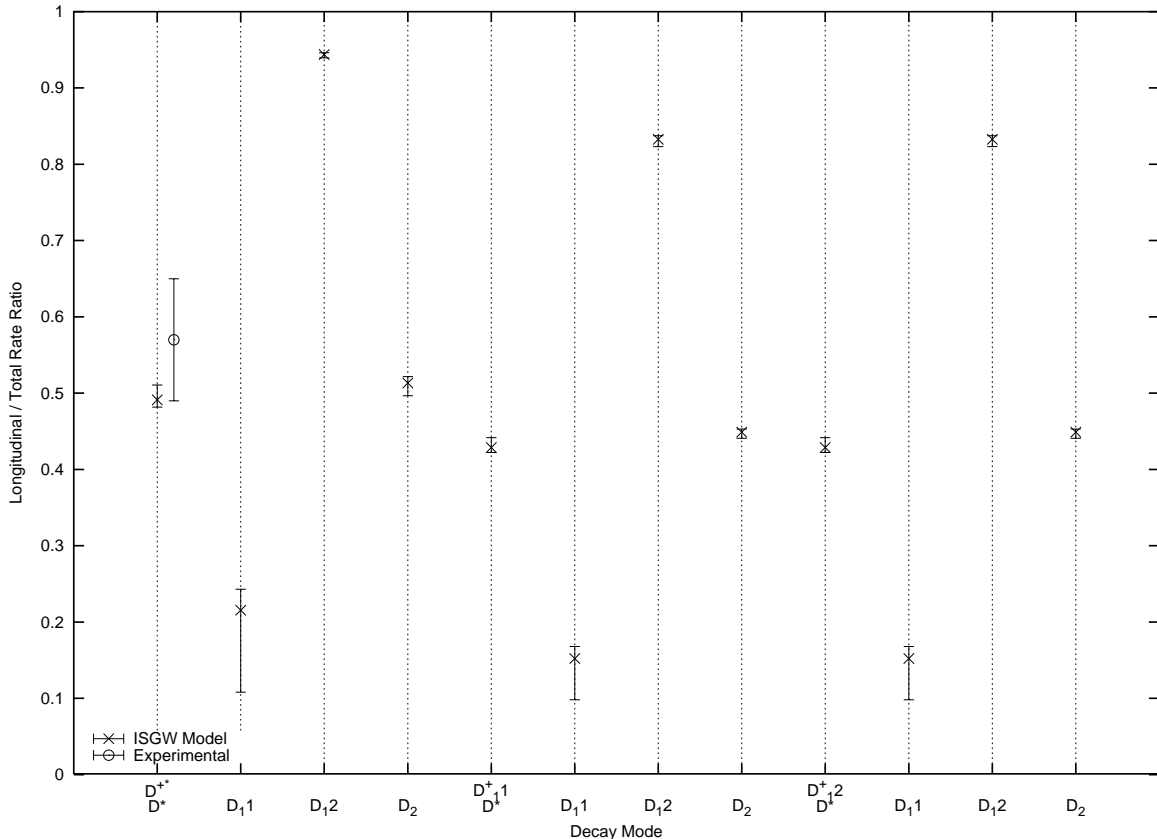
FIG. 7: Polarization Ratios: ISGW model and experimental values. See the text for references to experimental results.

given by:

$$|D_{s1}\rangle = \sin\phi \left|{}^3P_1\right\rangle + \cos\phi \left|{}^1P_1\right\rangle, \qquad (13)$$
$$|D'_{s1}\rangle = \cos\phi \left|{}^3P_1\right\rangle - \sin\phi \left|{}^1P_1\right\rangle. \qquad (14)$$

When $\phi = 0$: D_{s1} is purely ${}^1P_1$ and corresponds to our $D_{s1}2$, and D'_{s1} is purely ${}^3P_1$ and corresponds to our $D_{s1}1$. In the heavy quark limit the physical states are ${}^{3/2}1^+$ and ${}^{1/2}1^+$ (${}^j J^P$ j-j coupling eigenstates) corresponding to $\phi = -54.7°$.

Plots of branching ratios to these mesons and D and D^* as a function of ϕ are shown in Figures 8 and 9 respectively. We have ignored the mass difference and assumed the $D_s(2460)$ to be a conventional scalar meson. In our conventions the decay constants of the ${}^3P_1$ and ${}^1P_1$ axials have opposite sign (see Appendix F) and this must be taken in to account when calculating the amplitudes. The estimated experimental limits are shown. Because only limits exist it is not yet possible to determine the mixing angle using these decays. With measured branching ratios these decays provide a relatively clean way to measure the mixing angle but dependent on the D_{s1} decay constants.

Datta and O'Donnell [10] claim that there is a discrepancy between experiment and theory. However they only consider ratios of decay constants and ignore the mass differences between the s and p-wave mesons. Here we have shown that if the ISGW model is used and the mass differences are taken in to account there is no inconsistency between experiment and theory.

Ignoring effects due to the different masses between the ${}^3P_1$ and ${}^1P_1$ axial vector mesons, the only difference in branching ratios is due to the decay constants. The quark model expressions for decay constants given in Appendix F imply that the branching ratio to ${}^3P_1$ D_s is larger than that to ${}^1P_1$ D_s because the first is proportional to the reduced mass whereas the later is proportional to the inverse of the difference of inverse masses. In the equal quark mass limit only the ${}^3P_1$ meson can be produced, not the ${}^1P_1$. In the heavy quark limit only the ${}^{1/2}1^+$ meson can be produced, not the ${}^{3/2}1^+$ as remarked in Ref. [40].

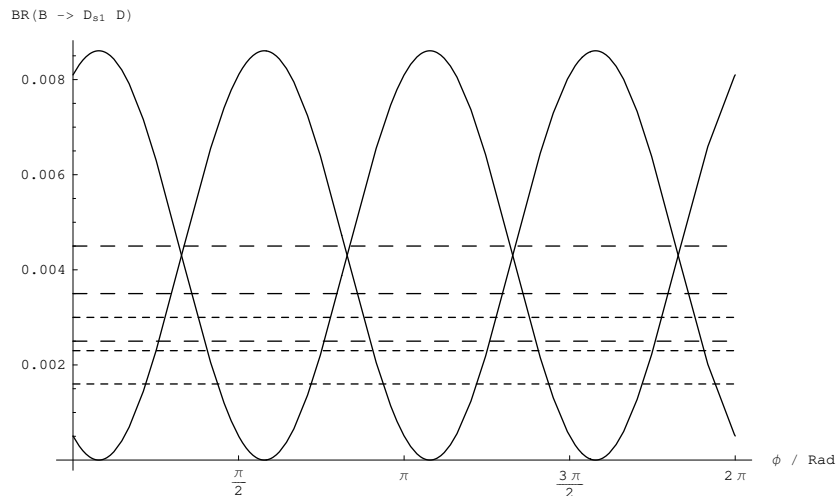The axials and vectors can not be compared to the

BR(B -> D_{s1} D)

FIG. 8: Branching Ratios to $D_{s1}\,D$ as a function of mixing angle. At $\phi = 0$ the top curve is D'_{s1} and the lower curve is D_{s1}. The experimental lower limits with 1σ errors are shown for B^+ (finer dashing) and scaled B^0 (coarser dashing).

BR(B -> D_{s1} D*)
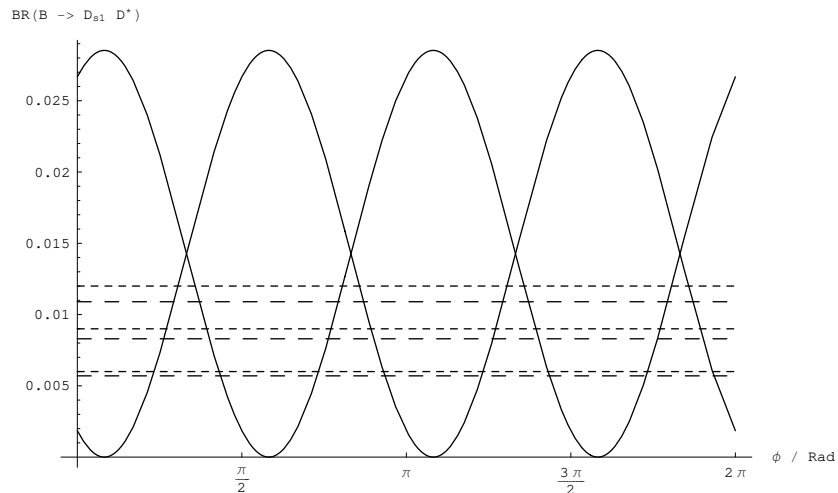
FIG. 9: Branching Ratios to $D_{s1}\,D^*$ as a function of mixing angle. At $\phi = 0$ the top curve is D'_{s1} and the lower curve is D_{s1}. The experimental lower limits with 1σ errors are shown for B^+ (finer dashing) and scaled B^0 (coarser dashing).

scalars and pseudoscalars as simply. This is because the amplitudes involve different combinations of form factors as seen in Appendix C.

VI. CONCLUSIONS

The ISGW model with the factorization hypothesis produces robust predictions for branching ratios and polarization fractions for the $B \to D_s D$ decays, which are in general agreement with the limited experimental data. The predictions are also in line with those from BSW, HQET and pole models. We have made predictions for

all combinations of s and p-wave final state mesons that can be measured in B decays. There are opportunities to probe the nature of the $D_s(2317)$ and $D_s(2460)$ states and determine the axial vector meson mixing using these decays. Measuring more polarization fractions will be interesting because they weigh different form factors at the same momentum transfer. This method has also be used to calculate branching ratios and polarization fractions in $B \to DD$ decays.

With the B factories at BABAR and Belle, the Tevatron and later LHCb, more precise data and also data on other decay modes should emerge.

It is important to note that these approximations are

robust for the generic class of $D_s\,D$ decays but are more suspect for color suppressed $B \to J/\psi K$ (and excited) decays. These are outside the kinematically valid region and experimental data on these modes disagree with results from this model. In addition, the factorization hypothesis fails for these decays as evidenced by the observation of a $\chi_{c0}\,K^+$ decay mode at BABAR [41] and Belle [42]. A possible contribution to these discrepancies could be final state rescattering of $(c\bar{s})\,(u\bar{c})$ in to $(c\bar{c})\,(u\bar{s})$ final states [43].

[1] N. Isgur, D. Scora, B. Grinstein, and M. B. Wise, Phys. Rev. **D39**, 799 (1989).

[2] Z. Luo and J. L. Rosner, Phys. Rev. **D64**, 094001 (2001), hep-ph/0101089.

[3] D. Scora and N. Isgur, Phys. Rev. **D52**, 2783 (1995), hep-ph/9503486.

[4] M. Wirbel, B. Stech, and M. Bauer, Z. Phys. **C29**, 637 (1985).

[5] M. Bauer, B. Stech, and M. Wirbel, Z. Phys. **C34**, 103 (1987).

[6] C. W. Bauer, S. Fleming, D. Pirjol, and I. W. Stewart, Phys. Rev. **D63**, 114020 (2001), hep-ph/0011336.

[7] V. L. Chernyak and I. R. Zhitnitsky, Nucl. Phys. **B345**, 137 (1990).

[8] V. M. Belyaev, A. Khodjamirian, and R. Ruckl, Z. Phys. **C60**, 349 (1993), hep-ph/9305348.

[9] C.-H. Chen, C.-Q. Geng, and Z.-T. Wei, (2005), hep-ph/0507295.

[10] A. Datta and P. J. O'Donnell, Phys. Lett. **B572**, 164 (2003), hep-ph/0307106.

[11] H.-Y. Cheng, C.-K. Chua, and C.-W. Hwang, Phys. Rev. **D69**, 074025 (2004), hep-ph/0310359.

[12] H.-Y. Cheng, Phys. Rev. **D68**, 094005 (2003), hep-ph/0307168.

[13] M. Beneke, G. Buchalla, M. Neubert, and C. T. Sachrajda, Phys. Rev. Lett. **83**, 1914 (1999), hep-ph/9905312.

[14] M. Beneke, G. Buchalla, M. Neubert, and C. T. Sachrajda, Nucl. Phys. **B591**, 313 (2000), hep-ph/0006124.

[15] M. Beneke and M. Neubert, Nucl. Phys. **B675**, 333 (2003), hep-ph/0308039.

[16] D. Bortoletto and S. Stone, Phys. Rev. Lett. **65**, 2951 (1990).

[17] C. Hayne and N. Isgur, Phys. Rev. **D25**, 1944 (1982).

[18] J. J. Dudek, *Phenomenology of Exotic Hadrons - Hybrid Mesons and Pentaquarks*, PhD thesis, Rudolf Peierls Centre for Theoretical Physics, Department of Physics, Universisty of Oxford, 2004.

[19] S. Capstick and S. Godfrey, Phys. Rev. **D41**, 2856 (1990).

[20] F. E. Close and J. J. Dudek, Phys. Rev. **D69**, 034010 (2004), hep-ph/0308098.

[21] M. Neubert and B. Stech, Adv. Ser. Direct. High Energy Phys. **15**, 294 (1998), hep-ph/9705292.

[22] S. Veseli and I. Dunietz, Phys. Rev. **D54**, 6803 (1996), hep-ph/9607293.

[23] Particle Data Group, S. Eidelman *et al.*, Phys. Lett. **B592**, 1 (2004).

[24] K. Abe *et al.*, (2005), hep-ex/0508040.

[25] BaBar, B. Aubert *et al.*, Phys. Rev. **D71**, 091104 (2005), hep-ex/0502041.

[26] BABAR, B. Aubert *et al.*, Phys. Rev. Lett. **93**, 181801 (2004), hep-ex/0408041.

[27] Belle, P. Krokovny *et al.*, Phys. Rev. Lett. **91**, 262002 (2003), hep-ex/0308019.

[28] Particle Data Group, S. Eidelman *et al.*, Phys. Lett. **B592**, 1 (2004), 2005 partial update for the 2006 edition available on the PDG WWW pages (URL: http://pdg.lbl.gov/).

[29] E. S. Swanson, Ann. Phys. **220**, 73 (1992).

[30] Private communication with Eric Swanson.

[31] M. Okamoto, PoS **LAT2005**, 013 (2005), hep-lat/0510113.

[32] S. Hashimoto, A. S. Kronfeld, P. B. Mackenzie, S. M. Ryan, and J. N. Simone, Phys. Rev. **D66**, 014503 (2002), hep-ph/0110253.

[33] CLEO, M. Artuso *et al.*, Phys. Rev. Lett. **95**, 251801 (2005), hep-ex/0508057.

[34] Belle, H. Miyake *et al.*, Phys. Lett. **B618**, 34 (2005), hep-ex/0501037.

[35] G. Majumder *et al.*, (2005), hep-ex/0502038.

[36] BaBar, B. Aubert *et al.*, Phys. Rev. Lett. **95**, 151804 (2005), hep-ex/0506082.

[37] F. E. Close and E. S. Swanson, Phys. Rev. **D72**, 094004 (2005), hep-ph/0505206.

[38] W. A. Bardeen, E. J. Eichten, and C. T. Hill, Phys. Rev. **D68**, 054024 (2003), hep-ph/0305049.

[39] T. Barnes, F. E. Close, and H. J. Lipkin, Phys. Rev. **D68**, 054006 (2003), hep-ph/0305025.

[40] A. Le Yaouanc, L. Oliver, O. Pene, and J. C. Raynal, Phys. Lett. **B387**, 582 (1996), hep-ph/9607300.

[41] BABAR, B. Aubert *et al.*, Phys. Rev. **D69**, 071103 (2004), hep-ex/0310015.

[42] Belle, K. Abe *et al.*, Phys. Rev. Lett. **88**, 031802 (2002), hep-ex/0111069.

[43] F. E. Close, E. S. Swanson, and C. E. Thomas, Paper in preparation.

[44] There are many definitions in the literature. Note that here we use the same conventions for vector and axial vector mesons.

[45] Again there are many different conventions here. We use the same convention for scalar and pseudoscalar mesons.

APPENDIX A: GENERAL PARAMETERIZATION OF VECTOR-AXIAL CURRENTS BETWEEN MESONS

When X is a pseudoscalar $^1S_0$ 0^{-+}:

$$\langle X \left| V_\mu \right| B \rangle \equiv f_+ (P_B + P_X)_\mu + f_- (P_B - P_X)_\mu. \tag{A1}$$

When X is a vector $^3S_1$ 1^{--} with polarization vector ϵ_μ:

$$\langle X \left| A_\mu \right| B \rangle \equiv f \epsilon_\mu^* + a_+ (\epsilon^* \cdot P_B)(P_B + P_X)_\mu + a_- (\epsilon^* \cdot P_B)(P_B - P_X)_\mu, \tag{A2}$$

$$\langle X \left| V_\mu \right| B \rangle \equiv i g \epsilon_{\mu\nu\rho\sigma} \epsilon^{*\nu} (P_B + P_X)^\rho (P_B - P_X)^\sigma. \tag{A3}$$

When X is a scalar $^3P_0$ 0^{++}:

$$\langle X \left| A_\mu \right| B \rangle \equiv u_+ (P_B + P_X)_\mu + u_- (P_B - P_X)_\mu. \tag{A4}$$

When X is an axial vector $^3P_1$ 1^{++} with polarization vector ϵ_μ:

$$\langle X \left| V_\mu \right| B \rangle \equiv l \epsilon_\mu^* + c_+ (\epsilon^* \cdot P_B)(P_B + P_X)_\mu + c_- (\epsilon^* \cdot P_B)(P_B - P_X)_\mu, \tag{A5}$$

$$\langle X \left| A_\mu \right| B \rangle \equiv i q \epsilon_{\mu\nu\rho\sigma} \epsilon^{*\nu} (P_B + P_X)^\rho (P_B - P_X)^\sigma. \tag{A6}$$

When X is an axial vector $^1P_1$ 1^{+-} with polarization vector ϵ_μ:

$$\langle X \left| V_\mu \right| B \rangle \equiv r \epsilon_\mu^* + s_+ (\epsilon^* \cdot P_B)(P_B + P_X)_\mu + s_- (\epsilon^* \cdot P_B)(P_B - P_X)_\mu, \tag{A7}$$

$$\langle X \left| A_\mu \right| B \rangle \equiv i v \epsilon_{\mu\nu\rho\sigma} \epsilon^{*\nu} (P_B + P_X)^\rho (P_B - P_X)^\sigma, \tag{A8}$$

When X is a tensor $^3P_2$ 2^{++} with polarization tensor $\epsilon_{\mu\nu}$:

$$\langle X \left| A_\mu \right| B \rangle \equiv k \epsilon_{\mu\nu}^* P_B^\nu + b_+ (\epsilon_{\alpha\beta}^* P_B^\alpha P_B^\beta)(P_B + P_X)_\mu + b_- (\epsilon_{\alpha\beta}^* P_B^\alpha P_B^\beta)(P_B - P_X)_\mu, \tag{A9}$$

$$\langle X \left| V_\mu \right| B \rangle \equiv i h \epsilon_{\mu\nu\lambda\rho} \epsilon^{*\nu\alpha} P_{B\alpha} (P_B + P_X)^\lambda (P_B - P_X)^\rho. \tag{A10}$$

APPENDIX B: POLARIZATION VECTORS FOR $J = 1$ AND $J = 2$ MESONS

For a vector meson with 4-momentum $(E, 0, 0, |\mathbf{q}|)$ and mass M the polarization vectors are

$$\epsilon_+^\mu = -\frac{1}{\sqrt{2}}(0, 1, i, 0), \tag{B1}$$

$$\epsilon_-^\mu = \frac{1}{\sqrt{2}}(0, 1, -i, 0), \tag{B2}$$

$$\epsilon_L^\mu = \frac{1}{M}(|\mathbf{q}|, 0, 0, E). \tag{B3}$$

For a vector meson with 4-momentum $(E, 0, 0, -|\mathbf{q}|)$ and mass M the polarization vectors (in the spin rather than the helicity basis) are

$$\epsilon_+^\mu = -\frac{1}{\sqrt{2}}(0, 1, i, 0), \tag{B4}$$

$$\epsilon_-^\mu = \frac{1}{\sqrt{2}}(0, 1, -i, 0), \tag{B5}$$

$$\epsilon_L^\mu = \frac{1}{M}(-|\mathbf{q}|, 0, 0, E). \tag{B6}$$

For a tensor meson with 4-momentum $(E, 0, 0, |\mathbf{q}|)$ and

mass M the polarization tensors can be obtained by taking the outer product of two spin-1 polarization vectors with the appropriate Clebsh-Gordon coefficients. The polarization tensors are given by:

$$\epsilon^{\mu\nu}_{++} = \frac{1}{2} \begin{bmatrix} 0 & 0 & 0 & 0 \\ 0 & 1 & i & 0 \\ 0 & i & -1 & 0 \\ 0 & 0 & 0 & 0 \end{bmatrix}, \tag{B7}$$

$$\epsilon^{\mu\nu}_{+} = -\frac{1}{2M} \begin{bmatrix} 0 & |\mathbf{q}| & i|\mathbf{q}| & 0 \\ |\mathbf{q}| & 0 & 0 & E \\ i|\mathbf{q}| & 0 & 0 & iE \\ 0 & E & iE & 0 \end{bmatrix}, \tag{B8}$$

$$\epsilon^{\mu\nu}_{0} = \sqrt{\frac{2}{3}} \begin{bmatrix} \frac{|\mathbf{q}|^2}{M^2} & 0 & 0 & \frac{|\mathbf{q}|E}{M^2} \\ 0 & -\frac{1}{2} & 0 & 0 \\ 0 & 0 & -\frac{1}{2} & 0 \\ \frac{|\mathbf{q}|E}{M^2} & 0 & 0 & \frac{E^2}{M^2} \end{bmatrix}, \tag{B9}$$

$$\epsilon^{\mu\nu}_{-} = \frac{1}{2M} \begin{bmatrix} 0 & |\mathbf{q}| & -i|\mathbf{q}| & 0 \\ |\mathbf{q}| & 0 & 0 & E \\ -i|\mathbf{q}| & 0 & 0 & -iE \\ 0 & E & -iE & 0 \end{bmatrix}, \tag{B10}$$

$$\epsilon^{\mu\nu}_{--} = \frac{1}{2} \begin{bmatrix} 0 & 0 & 0 & 0 \\ 0 & 1 & -i & 0 \\ 0 & -i & -1 & 0 \\ 0 & 0 & 0 & 0 \end{bmatrix}. \tag{B11}$$

APPENDIX C: POLARIZATION AMPLITUDES IN TERMS OF FORM FACTORS

For a pseudoscalar B decaying to a pseudoscalar (X) and a pseudoscalar (Y) the amplitude is given by

$$A = if_Y \left[\left(M_B^2 - M_X^2 \right) f_+ + M_Y^2 f_- \right]. \tag{C1}$$

For a decay in to a vector (X) and a pseudoscalar (Y) only a longitudinal vector is allowed and the amplitude is given by

$$A_L = -i \frac{f_Y |\mathbf{q}| M_B}{M_X} \left[f + a_+ (M_B^2 - M_X^2) + a_- M_Y^2 \right]. \tag{C2}$$

For a decay in to a pseudoscalar (X) and a vector (Y) only a longitudinal vector is allowed and the amplitude is given by

$$A_L = -2 f_Y f_+ |\mathbf{q}| M_B. \tag{C3}$$

For a decay in to a vector (X) and a vector (Y) the polarizations amplitudes for X positive, negative and longitudinal polarization respectively are

$$A_{+-} = -f_Y M_Y \left(f + 2g|\mathbf{q}| M_B \right), \tag{C4}$$

$$A_{-+} = -f_Y M_Y \left(f - 2g|\mathbf{q}| M_B \right), \tag{C5}$$

$$A_{ll} = \frac{f_Y}{M_X} \left[f \left(|\mathbf{q}|^2 + \frac{1}{4M_B^2} (M_B^2 + M_X^2 - M_Y^2)(M_B^2 + M_Y^2 - M_X^2) \right) + 2a_+ |\mathbf{q}|^2 M_B^2 \right], \tag{C6}$$

$$= \frac{f_Y}{M_X} \left[f P_Y . P_X + 2a_+ |\mathbf{q}|^2 M_B^2 \right]. \tag{C7}$$

For a decay in to a tensor (X) and a pseudoscalar (Y) only a longitudinally polarized tensor is allowed and the amplitude is given by

$$A_L = -i f_Y \left[k + b_+ (M_B^2 - M_X^2) + b_- M_Y^2 \right] \sqrt{\frac{2}{3}} \frac{M_B^2 |\mathbf{q}|^2}{M_X^2}. \tag{C8}$$

For a decay in to a tensor (X) and a vector (Y) the tensor can not have polarization ± 2. The polarization amplitudes for X positive, negative and longitudinally polarized respectively are given by

$$A_{+-} = -f_Y \frac{M_B |\mathbf{q}| M_Y}{M_X \sqrt{2}} \left(k + 2h M_B |\mathbf{q}| \right), \tag{C9}$$

$$A_{-+} = -f_Y \frac{M_B |\mathbf{q}| M_Y}{M_X \sqrt{2}} \left(k - 2h M_B |\mathbf{q}| \right), \tag{C10}$$

$$A_{ll} = \sqrt{\frac{2}{3}} \frac{|\mathbf{q}| M_B f_Y}{M_X^2} \left[k \left(|\mathbf{q}|^2 + \frac{1}{4 M_B^2} (M_B^2 + M_X^2 - M_Y^2)(M_B^2 + M_Y^2 - M_X^2) \right) + 2 M_B^2 |\mathbf{q}|^2 b_+ \right]. \tag{C11}$$

From these expressions it can be seen that the parity violation arises from a non-zero form factors g and h.

Amplitudes for when Y is an axial vector or scalar can be obtained simply by using the correct decay constant. Amplitudes when X is an axial vector or scalar can be obtained by replacing the vector or pseudoscalar form factors by the analogous axial or scalar ones given in Appendix A *and multiplying by -1 to account for the difference in sign of the vector and axial currents in V-A.*

APPENDIX D: ISGW FORM FACTORS FOR HARMONIC OSCILLATOR WAVEFUNCTIONS

We define:

$$\beta_{BX}^2 \equiv \frac{1}{2}(\beta_B^2 + \beta_X^2), \tag{D1}$$

$$\mu_\pm \equiv \left(\frac{1}{m_q} \pm \frac{1}{m_b} \right)^{-1}, \tag{D2}$$

and

$$F_n = \sqrt{\frac{\tilde{M}_X}{\tilde{M}_B}} \left(\frac{\beta_B \beta_X}{\beta_{BX}^2} \right)^{n/2} \exp \left[-\left(\frac{m_{qi}^2}{4 \tilde{M}_X \tilde{M}_B} \right) \frac{t_m - t}{\kappa^2 \beta_{BX}^2} \right]. \tag{D3}$$

The pseudoscalar ($^1S_0$) form factors are

$$f_+ = F_3 \left[1 + \frac{m_b}{2\mu_-} - \frac{m_b m_q m_{qi} \beta_B^2}{4\mu_+ \mu_- \tilde{M}_X \beta_{BX}^2} \right], \tag{D4}$$

$$f_- = F_3 \left[1 - (\tilde{M}_X + \tilde{M}_B) \left(\frac{1}{2m_q} - \frac{m_{qi} \beta_B^2}{4\mu_+ \tilde{M}_X \beta_{BX}^2} \right) \right]. \tag{D5}$$

The vector ($^3S_1$) form factors are

$$f = 2\tilde{M}_B F_3 \tag{D6}$$

$$g = \frac{1}{2} F_3 \left[\frac{1}{m_q} - \frac{m_{qi} \beta_B^2}{2\mu_- \tilde{M}_X \beta_{BX}^2} \right], \tag{D7}$$

$$a_+ = -\frac{F_3}{2\tilde{M}_X} \left[1 + \frac{m_{qi}}{m_b} \left(\frac{\beta_B^2 - \beta_X^2}{\beta_B^2 + \beta_X^2} \right) - \frac{m_{qi}^2 \beta_X^4}{4\mu_- \tilde{M}_B \beta_{BX}^4} \right], \tag{D8}$$

$$a_- = \frac{F_3}{2\tilde{M}_X} \left[1 - \frac{\tilde{M}_X}{\tilde{M}_B} + \frac{\tilde{M}_X^2}{m_q \tilde{M}_B} - \frac{\beta_B^2 m_{qi} \tilde{M}_X}{2\beta_{BX}^2 \tilde{M}_B \mu_+} \right]. \tag{D9}$$

The axial vector ($^1P_1$) form factors are

$$r = F_5 \frac{\tilde{M}_B \beta_B}{\sqrt{2} \mu_+}, \tag{D10}$$

$$v = F_5 \frac{\beta_B}{4\sqrt{2} m_b m_q}, \tag{D11}$$

$$s_+ = F_5 \frac{m_{qi}}{\sqrt{2} \tilde{M}_B \beta_B} \left[1 + \frac{m_b}{2\mu_-} - \frac{m_b m_q m_{qi} \beta_B^2}{4\mu_+ \mu_- \tilde{M}_X \beta_{BX}^2} \right], \tag{D12}$$

$$s_- = F_5 \frac{m_{qi}}{\sqrt{2} \tilde{M}_B \beta_B} \left[1 - \frac{\tilde{M}_X + \tilde{M}_B}{2m_q} + \frac{(\tilde{M}_X + \tilde{M}_B) \beta_B^2 m_{qi}}{4\mu_+ \beta_{BX}^2 \tilde{M}_X} \right]. \tag{D13}$$

Note the difference in v compared with B43 of [1], we have checked this and believe our expression is correct. We comment on this in Section III.

The scalar $(^3P_0)$ form factors are

$$u_+ = -F_5 \frac{m_b m_q m_{qi}}{\sqrt{6}\beta_B \tilde{M}_X \mu_-}, \tag{D14}$$

$$u_- = F_5 \frac{m_{qi}(\tilde{M}_X + \tilde{M}_B)}{\sqrt{6}\beta_B \tilde{M}_X}. \tag{D15}$$

Note the negative sign in u_+ compared with that in equation B37 of [1]. We comment on this in Section III.

The axial vector $(^3P_1)$ form factors are

$$q = F_5 \frac{m_{qi}}{2\tilde{M}_X \beta_B}, \tag{D16}$$

$$l = -F_5 \beta_B \tilde{M}_B \left[\frac{1}{\mu_-} + \frac{m_{qi}(t_m - t)}{2\tilde{M}_B \beta_B^2 \kappa^2} \left(\frac{1}{m_q} - \frac{m_{qi}\beta_B^2}{2\beta_{BX}\tilde{M}_X \mu_-} \right) \right], \tag{D17}$$

$$c_+ = F_5 \frac{m_{qi} m_b}{4\tilde{M}_B \beta_B \mu_-} \left[1 - \frac{m_{qi} m_q \beta_B^2}{2\tilde{M}_X \mu_- \beta_{BX}^2} \right], \tag{D18}$$

$$c_- = -F_5 \frac{m_{qi}(\tilde{M}_B + \tilde{M}_X)}{4\tilde{M}_B \beta_B} \left[\frac{1}{m_q} - \frac{m_{qi}\beta_B^2}{2\mu_- \beta_{BX}^2 \tilde{M}_X} \right]. \tag{D19}$$

The tensor $(^3P_2)$ form factors are

$$h = F_5 \frac{m_{qi}}{2\sqrt{2}\tilde{M}_B \beta_B} \left[\frac{1}{m_q} - \frac{m_{qi}\beta_B^2}{2\tilde{M}_X \mu_- \beta_{BX}^2} \right], \tag{D20}$$

$$k = \sqrt{2} F_5 \frac{m_{qi}}{\beta_B}, \tag{D21}$$

$$b_+ = -F_5 \frac{m_{qi}}{2\sqrt{2}\tilde{M}_X m_b \beta_B} \left[1 - \frac{m_{qi} m_b \beta_X^2}{2\mu_+ \tilde{M}_B \beta_{BX}^2} + \frac{m_{qi} m_b \beta_X^2}{4\tilde{M}_B \mu_- \beta_{BX}^2} \left(1 - \frac{m_{qi}\beta_X^2}{2\tilde{M}_B \beta_{BX}^2} \right) \right], \tag{D22}$$

$$b_- = F_5 \frac{m_{qi}}{2\sqrt{2}\tilde{M}_B^2 \beta_B} \left[-1 + \frac{\tilde{M}_X}{m_q} + \frac{\tilde{M}_B}{\tilde{M}_X} - \frac{m_{qi}}{\mu_+} + \frac{m_{qi}(\tilde{M}_X + \tilde{M}_B)}{2m_b m_q} \right]. \tag{D23}$$

APPENDIX E: ISGW FORM FACTORS FOR GENERAL WAVEFUNCTIONS

We define:

$$\beta_{BX}^2 \equiv \frac{1}{2}(\beta_B^2 + \beta_X^2), \tag{E1}$$

and

$$\mu_\pm \equiv \left(\frac{1}{m_q} \pm \frac{1}{m_b} \right)^{-1} \tag{E2}$$

In the following $\langle \rangle \equiv \langle X | B \rangle$ and $\langle O \rangle \equiv \langle X | O | B \rangle$. For example $\langle p_z \rangle = \int d^3 p . p_z . \psi^*(p)\psi(p)$. For notational convenience we include the common $\sqrt{\tilde{M}_X / \tilde{M}_B}$ factors in $\langle \rangle$ and $\langle O \rangle$.

The pseudoscalar $(^1S_0)$ form factors are

$$f_+ = \langle \rangle \left(1 + \frac{m_b}{2\mu_-} \right) + \frac{\langle p_z \rangle}{|\mathbf{q}|} \frac{m_b m_q}{2\mu_- \mu_+}, \tag{E3}$$

$$f_- = \langle \rangle \left(1 - \frac{\tilde{M}_X + \tilde{M}_B}{2m_q} \right) - \frac{\langle p_z \rangle}{|\mathbf{q}|} \frac{\tilde{M}_X + \tilde{M}_B}{2\mu_+}. \tag{E4}$$

The vector $(^3S_1)$ form factors are

$$g = \frac{1}{2} \left[\frac{\langle \rangle}{m_q} + \frac{\langle p_z \rangle}{|\mathbf{q}|\mu_-} \right], \tag{E5}$$

$$f = 2 \langle \rangle \tilde{M}_B, \tag{E6}$$

$$a_+ = -\frac{1}{2\tilde{M}_X} \left[\langle \rangle \left(1 + \frac{\tilde{M}_X}{\tilde{M}_B} - \frac{\tilde{M}_X^2}{m_q \tilde{M}_B} \right) - \frac{\langle p_z \rangle}{|\mathbf{q}|} \frac{\tilde{M}_X^2}{\tilde{M}_B \mu_+} \right], \tag{E7}$$

$$a_- = \frac{1}{2\tilde{M}_X} \left[\langle \rangle \left(1 - \frac{\tilde{M}_X}{\tilde{M}_B} + \frac{\tilde{M}_X^2}{m_q \tilde{M}_B} \right) + \frac{\langle p_z \rangle}{|\mathbf{q}|} \frac{\tilde{M}_X^2}{\tilde{M}_B \mu_+} \right]. \tag{E8}$$

The axial vector ($^1P_1$) form factors are

$$r = \langle p_+ \rangle \frac{\tilde{M}_B}{\mu_+}, \tag{E9}$$

$$v = \langle p_+ \rangle \frac{1}{4m_b m_q}, \tag{E10}$$

$$s_+ = \langle\rangle \frac{\tilde{M}_X}{|\mathbf{q}|\tilde{M}_B}\left(1 + \frac{m_b}{2\mu_-}\right) + \langle p_z \rangle \frac{m_b m_q \tilde{M}_X}{2\tilde{M}_B \mu_+ |\mathbf{q}|^2 \mu_-} - \langle p_+ \rangle \frac{1}{2\tilde{M}_B \mu_+}\left(1 + \frac{m_b m_q \tilde{M}_X}{\mu_- |\mathbf{q}|^2} + \frac{m_b m_q}{2\mu_- \tilde{M}_X}\right), \tag{E11}$$

$$s_- = \langle\rangle \frac{\tilde{M}_X}{|\mathbf{q}|\tilde{M}_B}\left(1 - \frac{(\tilde{M}_X + \tilde{M}_B)}{2m_q}\right) - \langle p_z \rangle \frac{\tilde{M}_X(\tilde{M}_X + \tilde{M}_B)}{2\tilde{M}_B \mu_+ |\mathbf{q}|^2} + \langle p_+ \rangle \frac{(\tilde{M}_X + \tilde{M}_B)\tilde{M}_X}{2\tilde{M}_B \mu_+ |\mathbf{q}|^2}. \tag{E12}$$

The scalar ($^3P_0$) form factors are

$$u_+ = -\langle\rangle \frac{1}{\sqrt{3}} \frac{m_b m_q}{|\mathbf{q}|\mu_-}, \tag{E13}$$

$$u_- = \langle\rangle \frac{1}{\sqrt{3}} \frac{(\tilde{M}_X + \tilde{M}_B)}{|\mathbf{q}|}. \tag{E14}$$

The axial vector ($^3P_1$) form factors are

$$q = \langle\rangle \frac{1}{\sqrt{2}|\mathbf{q}|}, \tag{E15}$$

$$l = -\frac{\tilde{M}_B}{\sqrt{2}}\left[\frac{\langle p_z \rangle}{\mu_-} + \frac{\langle\rangle |\mathbf{q}|}{m_q} + \frac{\langle p_+ \rangle}{\mu_-}\right], \tag{E16}$$

$$c_+ = \frac{m_b m_q \tilde{M}_X}{2\sqrt{2}\tilde{M}_B |\mathbf{q}|^2 \mu_-}\left[-\frac{\langle p_+ \rangle}{\mu_-} + \frac{\langle p_z \rangle}{\mu_-} + \frac{\langle\rangle |\mathbf{q}|}{m_q}\right], \tag{E17}$$

$$c_- = \frac{\tilde{M}_X(\tilde{M}_X + \tilde{M}_B)}{2\sqrt{2}\tilde{M}_B |\mathbf{q}|^2}\left[\frac{\langle p_+ \rangle}{\mu_-} - \frac{\langle p_z \rangle}{\mu_-} - \frac{\langle\rangle |\mathbf{q}|}{m_q}\right]. \tag{E18}$$

The tensor ($^3P_2$) form factors are

$$k = \langle\rangle \frac{2\tilde{M}_X}{|\mathbf{q}|}, \tag{E19}$$

$$h = \frac{\tilde{M}_X}{2\tilde{M}_B |\mathbf{q}|^2}\left[\frac{\langle p_z \rangle}{\mu_-} + \frac{\langle\rangle |\mathbf{q}|}{m_q} - \frac{\langle p_+ \rangle}{\mu_-}\right], \tag{E20}$$

$$b_+ = \frac{\tilde{M}_X^2}{2|\mathbf{q}|^2 \tilde{M}_B^2}\left[\langle p_z \rangle\left(\frac{1}{\mu_+} + \frac{1}{2\mu_-}\right) - \langle p_+ \rangle\left(\frac{1}{\mu_+} + \frac{1}{2\mu_-}\right) + |\mathbf{q}| \langle\rangle\left(\frac{1}{m_q} - \frac{2}{\tilde{M}_X} - \frac{m_b m_q}{\tilde{M}_X^2 \mu_-}\right)\right], \tag{E21}$$

$$b_- = \frac{\tilde{M}_X^2}{2|\mathbf{q}|^2 \tilde{M}_B^2}\left[\langle p_z \rangle\left(\frac{1}{\mu_+} - \frac{(\tilde{M}_X + \tilde{M}_B)}{2m_b m_q}\right) - \langle p_+ \rangle\left(\frac{1}{\mu_+} - \frac{(\tilde{M}_X + \tilde{M}_B)}{2m_b m_q}\right) + |\mathbf{q}| \langle\rangle\left(\frac{1}{m_q} - \frac{2}{\tilde{M}_X} + \frac{(\tilde{M}_B + \tilde{M}_X)}{\tilde{M}_X^2}\right)\right]. \tag{E22}$$

APPENDIX F: DECAY CONSTANTS IN THE QUARK MODEL

A non-relativistic quark model calculation using simple harmonic oscillator wavefunctions gives:

$$f_{^1P_0} = i\sqrt{2}\frac{N(Y)}{M_Y}, \tag{F1}$$

$$f_{^1P_1} = \sqrt{2}\frac{N(Y)}{M_Y}, \tag{F2}$$

$$f_{^3P_0} = -i\sqrt{3}\frac{\beta_Y N(Y)}{\mu_- M_Y}, \tag{F3}$$

$$f_{^3P_1} = -\sqrt{2}\frac{\beta_Y N(Y)}{\mu_+ M_Y}, \tag{F4}$$

$$f_{^1P_1} = \frac{\beta_Y N(Y)}{\mu_- M_Y}, \tag{F5}$$

$$f_{^3P_2} = 0. \tag{F6}$$

β_Y is the SHO wavefunction parameter,

$$N(Y) \propto (4\pi\beta_Y^2)^{\frac{3}{4}}\sqrt{M_Y}$$

and

$$\frac{1}{\mu_\pm} = \frac{1}{m_{q2}} \pm \frac{1}{m_{q1}}.$$

Here m_{q1} is the outgoing quark mass and m_{q2} is the outgoing antiquark mass. The sign of the $^3P_1$ decay constant depends on which way around the spin and orbital angular momentum are coupled. We use the convention consistent with the argument in Ref. [40]. In this work, a different relative sign here would only lead to the branching ratios shown in Figs. 8 & 9 being shifted in ϕ.

For general wavefunctions the above equations are replaced by:

$$f_{^1P_0} = i\sqrt{2}\frac{N(Y)}{M_Y} <0,0|0>_L, \tag{F7}$$

$$f_{^1P_1} = \sqrt{2}\frac{N(Y)}{M_Y} <0,0|0>_L, \tag{F8}$$

$$f_{^3P_0} = -i\frac{1}{\sqrt{6}}\frac{N(Y)}{\mu_- M_Y} (<1,0|p_z|0>_L + <1,1|p_+|0>_L + <1,-1|p_-|0>_L), \tag{F9}$$

$$f_{^3P_1} = -\frac{1}{2}\frac{N(Y)}{\mu_+ M_Y} (<1,1|p_+|0>_L + <1,-1|p_-|0>_L), \tag{F10}$$

$$f_{^1P_1} = \frac{1}{\sqrt{2}}\frac{N(Y)}{\mu_- M_Y} <1,0|p_z|0>_L, \tag{F11}$$

$$f_{^3P_2} = 0. \tag{F12}$$

Here the overlaps $<l,m_l|p_i|0>_L$ only contain the *spatial* integrals; the spin and Clebsh-Gordan factors have already been taken care of. $p_+ = -\frac{1}{\sqrt{2}}(p_x + ip_y)$ and $p_- = \frac{1}{\sqrt{2}}(p_x - ip_y)$.

Note that a tensor meson can not be produced from an axial-vector current.

In the equal mass limit $\frac{1}{\mu_-} = 0$ and so the scalar or $^1P_1$ axial can not be produced. However, the $^3P_1$ axial can be produced.

In the heavy quark limit where the quark mass $m_{q1} \to \infty$ and $\mu_- = \mu_+$ both axial vectors can be produced. It is useful to change from the L-S basis $^{2s+1}L_J$ to the j-j coupling basis $^jJ^P$ where j is the total angular momentum of the light degrees of freedom, J is the total angular momentum and P is the parity. The transformation is given by [40]:

$$|^1P_1\rangle = \sqrt{\frac{1}{3}}\left|^{1/2}1^+\right\rangle + \sqrt{\frac{2}{3}}\left|^{3/2}1^+\right\rangle \tag{F13}$$

$$|^3P_1\rangle = -\sqrt{\frac{2}{3}}\left|^{1/2}1^+\right\rangle + \sqrt{\frac{1}{3}}\left|^{3/2}1^+\right\rangle \tag{F14}$$

$$\left|^{3/2}1^+\right\rangle = \sqrt{\frac{2}{3}}|^1P_1\rangle + \sqrt{\frac{1}{3}}|^3P_1\rangle \tag{F15}$$

$$\left|^{1/2}1^+\right\rangle = \sqrt{\frac{1}{3}}|^1P_1\rangle - \sqrt{\frac{2}{3}}|^3P_1\rangle \tag{F16}$$

In the heavy quark limit $f_{^3P_1} = -\sqrt{2}f_{^1P_1}$ and so:

$$f_{3/2 1^+} = 0, \tag{F17}$$

$$f_{1/2 1^+} = \sqrt{3}f_{^1P_1}, \tag{F18}$$

$$f_{1/2 0^+} = -i\sqrt{3}f_{^1P_1}. \tag{F19}$$

So the $^{3/2}1^+$ axial can not be produced but the $^{1/2}1^+$ axial can. Note also that, apart from a phase, the scalar has the same decay constant. This is a specific realization of the general result given by Le Yaouanc et. al. in Ref. [40].

It is important to note that if it was the *antiquark* mass that was large there would be a relative negative sign between μ_- and μ_+ which would change the negative signs around in the basis change between L-S and j-j coupling. This means that the basis transformation has different signs in D_s^+ and D_s^- mesons.

APPENDIX G: TABLES OF RESULTS

Decay Mode	Branching Ratio	Lower	Upper
$D_s^*\, D$	1.49×10^{-2}	1.27×10^{-2}	1.70×10^{-2}
$D_s^*\, D^*$	3.18×10^{-2}	2.84×10^{-2}	3.50×10^{-2}
$D_s^*\, D_0$	6.97×10^{-4}	6.41×10^{-4}	7.36×10^{-4}
$D_s^*\, D_1 1$	1.54×10^{-3}	1.20×10^{-3}	1.70×10^{-3}
$D_s^*\, D_1 2$	2.20×10^{-3}	1.79×10^{-3}	2.51×10^{-3}
$D_s^*\, D_2$	1.34×10^{-3}	1.06×10^{-3}	1.54×10^{-3}
$D_{s1}1\, D$	8.10×10^{-3}	7.18×10^{-3}	8.92×10^{-3}
$D_{s1}1\, D^*$	2.67×10^{-2}	2.45×10^{-2}	2.88×10^{-2}
$D_{s1}1\, D_0$	2.70×10^{-4}	2.55×10^{-4}	2.84×10^{-4}
$D_{s1}1\, D_1 1$	6.82×10^{-4}	5.68×10^{-4}	7.25×10^{-4}
$D_{s1}1\, D_1 2$	7.17×10^{-4}	6.13×10^{-4}	7.88×10^{-4}
$D_{s1}1\, D_2$	5.07×10^{-4}	4.21×10^{-4}	5.61×10^{-4}
$D_{s1}2\, D$	5.07×10^{-4}	4.53×10^{-4}	5.53×10^{-4}
$D_{s1}2\, D^*$	1.86×10^{-3}	1.72×10^{-3}	2.00×10^{-3}
$D_{s1}2\, D_0$	1.48×10^{-5}	1.40×10^{-5}	1.55×10^{-5}
$D_{s1}2\, D_1 1$	3.79×10^{-5}	3.21×10^{-5}	4.00×10^{-5}
$D_{s1}2\, D_1 2$	3.84×10^{-5}	3.33×10^{-5}	4.18×10^{-5}
$D_{s1}2\, D_2$	2.61×10^{-5}	2.19×10^{-5}	2.87×10^{-5}
$D_s\, D$	1.76×10^{-2}	1.49×10^{-2}	2.05×10^{-2}
$D_s\, D^*$	7.51×10^{-3}	6.38×10^{-3}	8.88×10^{-3}
$D_s\, D_0$	4.63×10^{-4}	4.21×10^{-4}	4.94×10^{-4}
$D_s\, D_1 1$	2.16×10^{-4}	7.77×10^{-5}	2.67×10^{-4}
$D_s\, D_1 2$	2.76×10^{-3}	2.19×10^{-3}	3.20×10^{-3}
$D_s\, D_2$	3.21×10^{-4}	2.15×10^{-4}	3.92×10^{-4}
$D_{s0}\, D$	3.36×10^{-3}	2.97×10^{-3}	3.81×10^{-3}
$D_{s0}\, D^*$	1.28×10^{-3}	1.12×10^{-3}	1.50×10^{-3}
$D_{s0}\, D_0$	4.98×10^{-5}	4.64×10^{-5}	5.27×10^{-5}
$D_{s0}\, D_1 1$	1.57×10^{-5}	7.04×10^{-6}	1.87×10^{-5}
$D_{s0}\, D_1 2$	3.05×10^{-4}	2.49×10^{-4}	3.44×10^{-4}
$D_{s0}\, D_2$	2.44×10^{-5}	1.69×10^{-5}	2.91×10^{-5}

TABLE V: $B \rightarrow D_s D$ branching ratios calculated in the ISGW model. The branching ratio, lower and upper values give the average and range of results dependent on model choices as discussed in Section III.

Decay Mode	Longitudinal Polarization Fraction	Lower	Upper
$D_s^*\ D^*$	0.47	0.46	0.49
$D_s^*\ D_1 1$	0.19	0.10	0.22
$D_s^*\ D_1 2$	0.93	0.92	0.93
$D_s^*\ D_2$	0.50	0.48	0.50
$D_{s}1\ D^*$	0.42	0.42	0.44
$D_{s}1\ D_1 1$	0.15	0.10	0.16
$D_{s}1\ D_1 2$	0.81	0.80	0.82
$D_{s}1\ D_2$	0.44	0.44	0.45
$D_{s}2\ D^*$	0.41	0.41	0.43
$D_{s}2\ D_1 1$	0.15	0.11	0.16
$D_{s}2\ D_1 2$	0.76	0.75	0.77
$D_{s}2\ D_2$	0.43	0.43	0.44

TABLE VI: $B \rightarrow D_s D$ polarization fractions calculated in the ISGW model. The polarization fraction, lower and upper values give the average and range of results dependent on model choices as discussed in Section III.

Decay Mode	Branching Ratio	Lower	Upper
$D^{*+}\ D$	5.04×10^{-4}	4.26×10^{-4}	5.81×10^{-4}
$D^{*+}\ D^*$	9.58×10^{-4}	8.48×10^{-4}	1.06×10^{-3}
$D^{*+}\ D_0$	2.51×10^{-5}	2.29×10^{-5}	2.67×10^{-5}
$D^{*+}\ D_1 1$	5.29×10^{-5}	4.00×10^{-5}	5.90×10^{-5}
$D^{*+}\ D_1 2$	8.35×10^{-5}	6.71×10^{-5}	9.61×10^{-5}
$D^{*+}\ D_2$	4.70×10^{-5}	3.66×10^{-5}	5.45×10^{-5}
$D_1^+ 1\ D$	2.54×10^{-4}	2.24×10^{-4}	2.81×10^{-4}
$D_1^+ 1\ D^*$	7.93×10^{-4}	7.27×10^{-4}	8.58×10^{-4}
$D_1^+ 1\ D_0$	8.98×10^{-6}	8.45×10^{-6}	9.43×10^{-6}
$D_1^+ 1\ D_1 1$	2.24×10^{-5}	1.85×10^{-5}	2.39×10^{-5}
$D_1^+ 1\ D_1 2$	2.42×10^{-5}	2.06×10^{-5}	2.67×10^{-5}
$D_1^+ 1\ D_2$	1.71×10^{-5}	1.42×10^{-5}	1.91×10^{-5}
$D_1^+ 2\ D$	6.00×10^{-5}	5.30×10^{-5}	6.64×10^{-5}
$D_1^+ 2\ D^*$	1.88×10^{-4}	1.72×10^{-4}	2.03×10^{-4}
$D_1^+ 2\ D_0$	2.12×10^{-6}	2.00×10^{-6}	2.23×10^{-6}
$D_1^+ 2\ D_1 1$	5.30×10^{-6}	4.38×10^{-6}	5.66×10^{-6}
$D_1^+ 2\ D_1 2$	5.72×10^{-6}	4.86×10^{-6}	6.32×10^{-6}
$D_1^+ 2\ D_2$	4.05×10^{-6}	3.35×10^{-6}	4.51×10^{-6}
$D^+\ D$	7.95×10^{-4}	6.69×10^{-4}	9.36×10^{-4}
$D^+\ D^*$	3.46×10^{-4}	2.92×10^{-4}	4.12×10^{-4}
$D^+\ D_0$	2.36×10^{-5}	2.13×10^{-5}	2.54×10^{-5}
$D^+\ D_1 1$	1.19×10^{-5}	4.10×10^{-6}	1.48×10^{-5}
$D^+\ D_1 2$	1.39×10^{-4}	1.09×10^{-4}	1.62×10^{-4}
$D^+\ D_2$	1.72×10^{-5}	1.14×10^{-5}	2.12×10^{-5}
$D_0^+\ D$	3.44×10^{-4}	3.05×10^{-4}	3.88×10^{-4}
$D_0^+\ D^*$	1.29×10^{-4}	1.13×10^{-4}	1.50×10^{-4}
$D_0^+\ D_0$	4.73×10^{-6}	4.42×10^{-6}	5.01×10^{-6}
$D_0^+\ D_1 1$	1.42×10^{-6}	6.55×10^{-7}	1.68×10^{-6}
$D_0^+\ D_1 2$	2.89×10^{-5}	2.37×10^{-5}	3.25×10^{-5}
$D_0^+\ D_2$	2.19×10^{-6}	1.52×10^{-6}	2.60×10^{-6}

TABLE VII: $B \rightarrow DD$ branching ratios calculated in the ISGW model. The branching ratio, lower and upper values give the average and range of results dependent on model choices as discussed in Section III.

Decay Mode	Longitudinal Polarization Fraction	Lower	Upper
$D^{*+}\ D^*$	0.49	0.48	0.51
$D^{*+}\ D_1 1$	0.22	0.11	0.24
$D^{*+}\ D_1 2$	0.94	0.94	0.95
$D^{*+}\ D_2$	0.51	0.50	0.52
$D_1^+ 1\ D^*$	0.43	0.42	0.44
$D_1^+ 1\ D_1 1$	0.15	0.098	0.17
$D_1^+ 1\ D_1 2$	0.83	0.82	0.84
$D_1^+ 1\ D_2$	0.45	0.44	0.45
$D_1^+ 2\ D^*$	0.43	0.42	0.44
$D_1^+ 2\ D_1 1$	0.15	0.098	0.17
$D_1^+ 2\ D_1 2$	0.83	0.82	0.84
$D_1^+ 2\ D_2$	0.45	0.44	0.45

TABLE VIII: $B \to DD$ polarization fractions calculated in the ISGW model. The polarization fraction, lower and upper values give the average and range of results dependent on model choices as discussed in Section III.

Decay Mode	CP Odd Fraction, $R_\perp$	Lower	Upper
$D^{*+}\ D^*$	8.61×10^{-2}	7.93×10^{-2}	8.95×10^{-2}
$D^{*+}\ D_1 1$	4.55×10^{-1}	3.99×10^{-1}	6.15×10^{-1}
$D^{*+}\ D_1 2$	5.76×10^{-4}	5.69×10^{-4}	5.89×10^{-4}
$D^{*+}\ D_2$	5.82×10^{-2}	5.68×10^{-2}	5.90×10^{-2}
$D_1^+ 1\ D^*$	7.12×10^{-2}	6.65×10^{-2}	7.36×10^{-2}
$D_1^+ 1\ D_1 1$	5.00×10^{-1}	4.56×10^{-1}	6.05×10^{-1}
$D_1^+ 1\ D_1 2$	9.33×10^{-4}	9.32×10^{-4}	9.35×10^{-4}
$D_1^+ 1\ D_2$	3.62×10^{-2}	3.45×10^{-2}	3.71×10^{-2}
$D_1^+ 2\ D^*$	7.12×10^{-2}	6.65×10^{-2}	7.36×10^{-2}
$D_1^+ 2\ D_1 1$	5.00×10^{-1}	4.56×10^{-1}	6.05×10^{-1}
$D_1^+ 2\ D_1 2$	9.33×10^{-4}	9.32×10^{-4}	9.35×10^{-4}
$D_1^+ 2\ D_2$	3.62×10^{-2}	3.45×10^{-2}	3.71×10^{-2}

TABLE IX: $B \to DD$ CP odd fractions $R_\perp$ calculated in the ISGW model. The polarization fraction, lower and upper values give the average and range of results dependent on model choices as discussed in Section III.